Chapter 6

Transport in Ag_2Se

This chapter is principally about the thermoelectric performance of Ag_2Se near its phase transition. In the sample studied here the Hall carrier concentration does not differ measurably in the order and disordered phases; this fact considerably simplifies arguments based on band structure analysis. While many samples show similar behavior, other samples show a sharp increase in n_H in the disordered phase; the reason for this distinction remains unclear. Without any measured difference in band structure, the Seebeck and zT are enhanced in the ordered phase compared to the disordered.

This increase in zT is not easily explained using standard band-structure analysis (*e.g.*, BoltzTraP) [127]). In this chapter I will introduce super-ionics as thermoelectric materials and explain why they are of interest. Then I will provide a brief overview of the band structure modeling used for this thesis. After this I will present and analyze the transport data of Ag_2Se and argue that the difference in its properties above and below its phase transition are not easily explained by band structure modeling.

In the final chapter, after I have also presented the transport of Cu_2Se, I will develop an explanation for its physics on the basis of the phenomenology of order-disorder transitions [95] and Onsagers phenomenology of non-equilibrium thermodynamics [132]. I will suggest that these effects may occur broadly; it may be that the sudden transformation of the phase transition brings a more general effect into contrast.

6.1 Ion conducting thermoelectrics

Mixed ion-electron conductors (MIECs) are of recent and increased interest as thermoelectric materials [1, 199, 50, 133, 200, 206, 121, 30, 179, 185, 66, 45]. MIECs are materials that conduct both ions and electrons [167]. This is of course a very broad category that includes semiconductors and solid electrolytes. They can be subcategorized by the relative size of ionic conductivity (σ_i) and electronic conductivity (σ_e) with the physics varying substantially from the $\sigma_i \gg \sigma_e$ regime to the $\sigma_e \gg \sigma_i$ regime. In some materials such as solid oxides used in fuel cells, these regimes may be bridged in a single material under varying conditions of oxygen partial pressure and temperature.

Thermoelectric ion conductors operate entirely in the $\sigma_e \gg \sigma_i$ regime. This regime is inescapable unless an entirely new conception of what makes a good thermoelectric material is made as compared to what is studied now. A good thermoelectric is a heavily doped semi-conductor with a carrier concentration generally optimized at between $10^{18}\,\mathrm{cm}^{-3}$ and $10^{21}\,\mathrm{cm}^{-3}$ [180], and an electrical conductivity in the $10^4\,\mathrm{S/m}$ to $10^6\,\mathrm{S/m}$ regime in which the electronic (κ_e) and lattice (κ_L) portion of thermal conductivity are nearly the same. Super-ionics are by their phenomenological definition the best ionic conductors. They have ion conductivities that are similar to that of a liquid, $\approx 10^2\,\mathrm{S/m}$. Therefore even in the most extreme conceivable case an ion-conducting thermoelectric has σ_i less than 5% of σ_e.

Direct enhancement of thermoelectric material conductivity by adding ionic conduction is therefore impossible. Fortunately, this simplifies the measurement procedure for total thermal and electrical conductivity; the great care must be taken in making DC measurements of materials with two species with order of magnitude different diffusion timescales [167, 164, 165] can here be ignored. The principal consideration is that the electrodes are blocking to ions so that the ion conducting specie does not leave the material. Empirically the graphite blocker layer between thermocouple and electrode accomplished this purpose. When that layer was forgotten or broken through, the Niobium thermocouple wire used for the electrode developed a

fine metallic coating and was rendered useless.

The driver of recent interest in MIEC thermoelectrics has been their extremely low thermal conductivity. A principal problem of engineering good thermoelectric material is to find methods for scattering lattice vibrations (phonons) and thereby reduce κ_L without also scattering electrons and thereby reducing σ. In $Ag_2Se_{0.05}Te_{0.05}$ κ_L is only 0.5 W/mK at 400 K [50] and Ag_8GeTe_6has been reported as having a glass-like thermal conductivity of 0.25 W/mK at 300 K with only negligible contribution from electrons. Though these nobel metal chalcogenides are the subject of this thesis and in fact have a longer history as thermoelectric materials than is commonly appreciated [24], the driver of the recent interest in MIECs has been $\beta - Zn4Sb3$.

In 1997 Caillat *et al.* first synthesized $\beta - Zn4Sb3$ as a thermoelectric material [30]. They determined it to have a maximum zT of 1.3 at 670 K which at the time was the highest ever measured at that temperature. This was driven by a κ_L at or slightly above $0.65 W m^{-1} K^{-1}$ from $400K$ to $650K$. They determined this to be very close to the thermal conductivity of a glass in accordance with Cahills formalism [28, 29]. On the basis of crystallography Snyder *et al.* [179] suggested that this low κ_L was due to scattering off of disordered interstitals.

Density functional theory analysis by Toberer *et al.* [186] showed that the Zn interstitial sites were of almost identical energy to the ground state sites, with meta-stable pathways connecting them. Both a nearly isoenergetic interstitial site and meta-stable energetic pathways are considered necessary conditions for super-ionic conduction [87]. Tracer diffusion experiments confirmed Zn_4Sb_3 to have a liquid-like ion diffusivity with site hopping activation energy only 20% higher than that of AgI [35]. Zn_4Sb_3 is therefore a super-ionic thermoelectric material [21, 151].

Super-ionic materials are often written about as having a *molten* sub-lattice of conducting ions [22, 103]. As this analogy was coined in reference to the liquid-like diffusivity of the conducting ion ($10^{-5}\,cm^2/s$) and the enthalpy of formation comparable to that of their melt, [21, 22] care must be taken in extending it beyond its physical underpinnings. It has been suggested in two ways that the lattice thermal conductivity may have properties similar to that of a liquid: that they should show

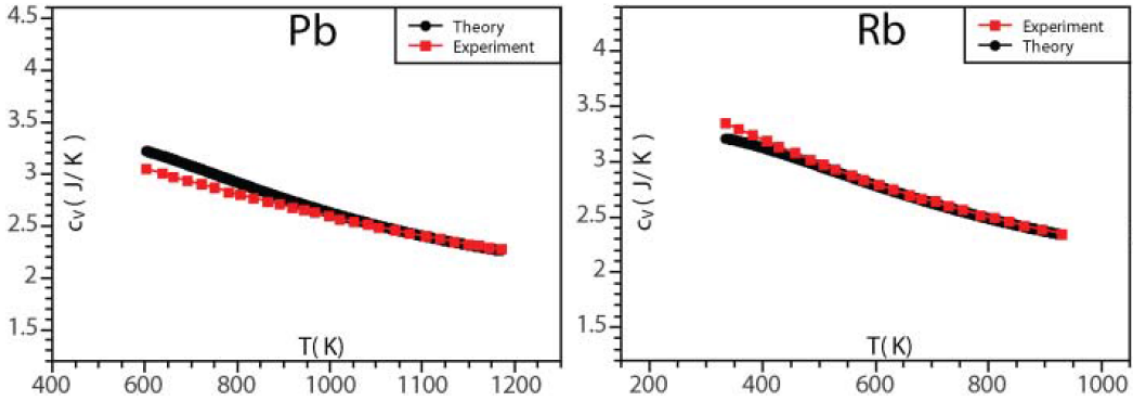

Figure 6.1: Heat capacity of liquid lead and rubidium with fit to theory. As temperature increases low frequence transverse modes disappear and thereby reduce c_V. Figure from Bolmatov *et al.* (2012) [17].

phonon softening due to coherent oscillations like a liquid [6], and that their constant volume heat capacity (c_V) should decrease with increasing temperature like a liquid [122, 189, 17].

The liquid-like heat capacity was proposed by Liu *et al.* in order to explain a decrease in c_P they observed above $800K$ in Cu_2Se [122]. While a solid has $c_V = 3k_b$, a liquid only has $c_V = 2k_b$ [189]. The solid heat capcity is due to the kinetic and potential energy contributions to heat capacity by the equipartition theorem. As in a mono-atomic gas, there are three degrees of freedom for position and momentum each and so c_v of a solid is $6 \times k_b/2 = 3k_b$. In a crytalline solid these contributions are split between two longitudinal and one transverse (or shear) propagation modes. A liquid is incapable of propagating all transverse oscillations and therefore loses the heat capacity associated with the potential energy of those modes (up to k_b).

In real liquids c_V is observed to decrease with temperature. Bolmatov *et al.* compiled data for twenty-one liquids showing this trend [17]. As an example, their data for Pb is shown in Figure 6.1. They model this trend as being due to two characteristic frequency. The first is the characteristic frequency of lattice oscillations, the Debye frequency (Ω_D). The second is the characteristic frequency of liquid hopping, which they call the Frenkel frequency (ω_F). Only shear modes with characteristic frequency ($\omega < \omega_F$) disappear. In this frequency regime the liquid atoms move fast enough to

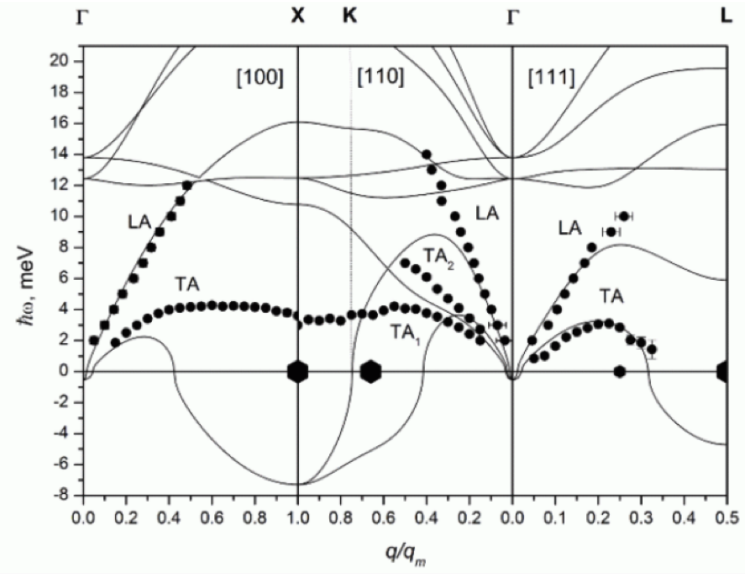

Figure 6.2: The fluctuations of ions between interstitial sites causes phonon mode to soften and scatter. In Zn_4Sb_3 Schwelka *et al.* [173] observed a strong anharmonic ratting of an Sb-dimer that they found could explain its anomalously low thermal conductivity. This behavior was found to effect the heat capacity even in the ordered phase, as evidenced by an Einstein peak in the heat capacity. If this behavior is a more general attribute of super-ionic materials in both their ordered and disordered phases, it may cause their low thermal conductivity. In his studies on single crystal $Cu_{1.8}Se$ Danilkin found substantial mode softening in $Cu_{1.8}Se$ [44].

damp out the oscillation. Above this frequency the liquid atoms move slow compared to the perturbation and so appear as a solid. As temperature increases more lattice vibration modes and ion hopping modes contribute to this behavior, with their contribution determined by the characteristic quantity. At $k_bT \gg \hbar\omega_D, \hbar\Omega_F$, the heat capacity simplifies to:

$$c_v = k_b \left(3 - \left(\frac{\omega_F}{\omega_D}\right)^3\right) \tag{6.1}$$

From inelastic neutron scattering measurements, the Frenkel timescale of Cu_2Se is 1 picosecond at 430K [42]. This corresponds to a $c_v = 2.98k_b$. Though this casts doubts on the explanation of Liu *et al.* [122], this author is unaware of any experiments showing the ion hop time of Cu_2Se at high temperature. One should also not discount the possibility that another material may show liquid-like reduction in its heat capacity much more strongly than Cu_2Se does.

While the liquid-like fluctuations of ions may not eliminate phonon propagation modes, they may scatter them. Ultra-sonic attenuation is a common feature of many solid electrolytes [3]. The theoretical explanations of Aniya for this behavior treats the mobile ions as a liquid free to move through out the lattice and thereby collide with the mobile cores [6]. A treatment of this class of materials that ignores the significant portion of ion life-time spent between interstitial sites [87] may not be able to fully capture their behavior.

6.2 Band Structure Modeling

In order to understand how Ag_2Se may have enhanced thermoelectric performance as compared to predictions based on its band structure, a brief overview of the relationship between band structure and Seebeck coefficient is necessary.

The electronic transport properties of heavily doped thermoelectrics can be typically described by modeling their electronic band structures [180, 127]. If the full electronic band structure is known — or more realistically predicted by density func-

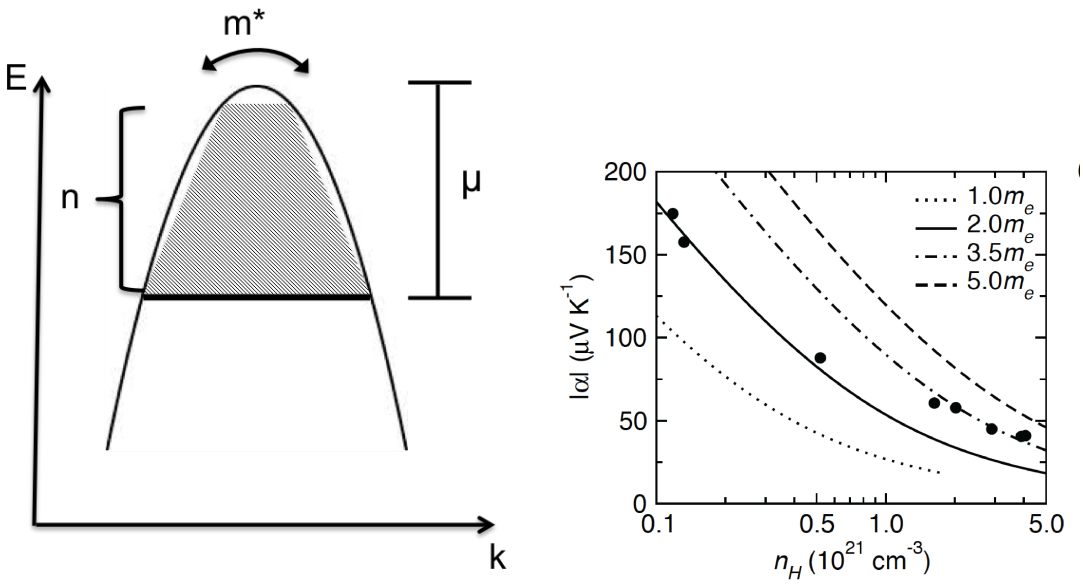

Figure 6.3: Left: Example of a single parabolic band. The band shown is a valence band as for a p-type conductor. The effective mass (m^*) determines the curvature of the band. The carrier concentration is the number of carriers between the band edge and the Fermi level.
Right: Example α versus n_H or *Pisarenko* plot. As m^* increases at constant n_H, α increases.

tional theory — then the transport coefficients could be computationally determined (*e.g.*, by BoltzTRaP [127]). However, simplified models that take into account only part of the band structure are extremely successful at predicting transport properties [154]. These models are successful because only band states within $3k_bT$ of the electron chemical potential (*i.e.*, the Fermi level) contribute significantly to electron transport [128]. The starting point for these models is the single parabolic band [170]. Thermoelectrics are heavily but not metallically doped, so that the band of the dominant conductor tends to dominate, but the Fermi level is not far from the band edge. A single parabolic band (SPB) has a dispersion relationship of form:

$$E = \frac{\hbar^2(k - k_0)^2}{2m^*} \tag{6.2}$$

This structure is shown in Figure 6.3(a). The effective mass (m^*) is typically given in units of electron masses (m_e). A heavier band (large m^*) has a low rate of curvature

of E with respect to k; increasing k increases E only slightly. In a light band (small m^*) increasing k increases E significantly.

If m^* and the band chemical potential (μ) are known, than the carrier concentration may be written as:

$$n = 4\pi \left(\frac{2m^* k_b T}{h^2} \right)^{3/2} F_{1/2}(\eta), \tag{6.3}$$

in which h is Plancks constant, $\eta = \frac{\mu}{k_b T}$ is the *reduced chemical potential* and $F_j(\eta)$ is the Fermi integral of order j.

If the energy dependence of scattering (λ) is also known, than transport variables may be modeled as well. In the case of scattering by acoustic phonons $\lambda = 0$. This is a good assumption for thermoelectric materials above the Debye temperature. In this model the Seebeck coefficient may be expressed as:

$$\alpha = \frac{k_b}{e} \left(\frac{(2+\lambda)F_{\lambda+1}}{(1+\lambda)F_\lambda} - \eta \right) \tag{6.4}$$

The general behavior can be understood well if the degenerate (*e.g.*, metallic) limit of Equation 6.4 is taken.

$$\alpha = \frac{\pi^{8/3} k_b^2}{3qh^2} n^{-2/3} T m^* (1+\lambda) \tag{6.5}$$

The inverse dependence of Seebeck on n argued for generally in the introduction is again present. Notably increased m^* results in increased Seebeck coefficient. This can be explained by a two step argument. A heavy band will have a lower η for the same n compared with a light band. A lower *eta* results in a larger Seebeck coefficient by equation 6.4. This effect is depicted in Figure 6.3(a) by means of a Pisarenko (α versus n or n_H) plot.

6.3 Prior Work on Ag_2Se

As established in Chapter 5 Ag_2Se shows a first order transition at 408 K as seen in both crystallography and calorimetry. Electronically Ag_2Se is a n-type material with high electron mobility and low thermal conductivity. These two attributes in combination give it promise as a high zT material near room temperature [1], but with two principal problems. The first is carrier concentration control, for which there is some uncontrolled effect in synthesis. The sample I will discuss below showed no carrier concentration shift through its phase transition, but many of the samples show a significant shift at that temperature [46]. The Seebeck coefficient of a second sample, produced by a different laboratory, shows the same trend as the sample principally studied here.

The second problem is hysteresis observed in transport properties in the low temperature phase and near the phase transition temperature [2]. These effects may be due to the kinetics of microstructural reorganization, as they appear in multiple materials. One example of this is $Ag_2Se_{0.5}Te_{0.5}$ [50]; other materials showed this effect but these instabilities rendered writing a meaningful publication on their thermoelectric performance impossible. In his paper on Ag_2Se my colleague Tristan Day applied band structure modeling to estimate the effective mass of the low temperature phase $0.2m_e$ and that of the high temperature phase to $0.3m_e$ [46].

6.4 Transport Measurements

Electrical conductivity (Figure 6.4(b)) was measured in the Van der Pauw geometry (see Chapter 2). Substantial hysteresis was observed both in the phase transition temperature and in the data in the low temperature phase. The data above the phase transition temperature is consistent on heating and on cooling. Though the data values on heating and cooling are inconsistent, the shape of the curves shows the same general trend. Above room temperature the conductivity linearly increases with temperature and then flattens out before the phase transition temperature. The

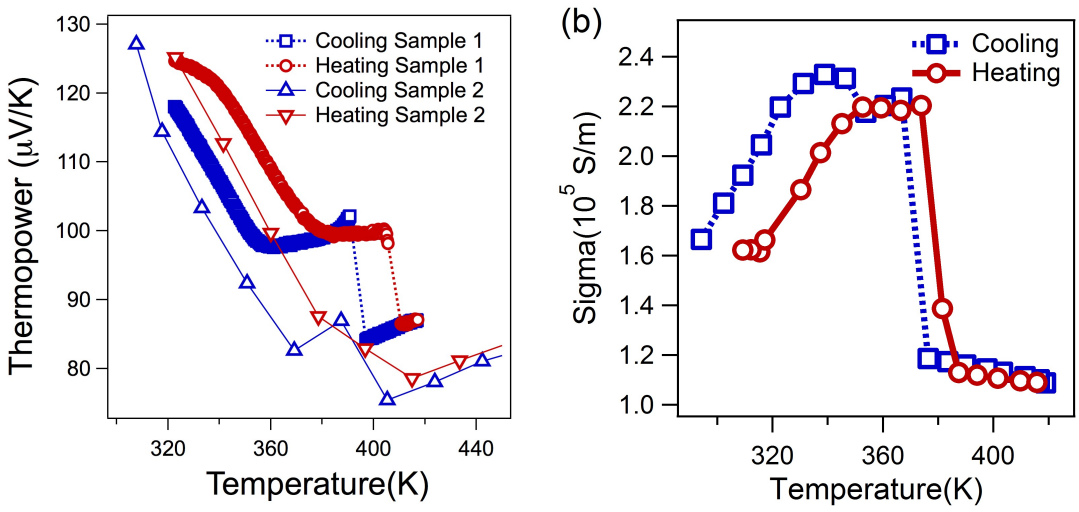

Figure 6.4: Seebeck Coefficient (a) and Electrical Conductivity of Ag_2Se measured on both heating and cooling.

conductivity drops by a factor of two at the phase transition temperature.

The Seebeck coefficent (Figure 6.4(a)) was measured by the ramp method discussed in Chapter 3 at 10 Kelvin per minute. It shows a similar behavior to the conductivity. At the temperatures at which the electrical conductivity increases, the Seebeck decreases. At the temperatures at which the electrical conductivity flattens, the Seebeck coefficient flattens. At the phase transitions it decreases slightly. During the phase transition the voltage versus ΔT data could not be fit to a line and so is not shown. The phase transition occurs at 405 K on heating and on 390 K on cooling. This hysteresis is expected for a first order phase transition. A second sample produced in a different lab by Dr. Fivos Drymiotis was measured by the oscillation method and showed a comparable change in the Seebeck coefficient through the phase transition.

The thermal diffusivity (figure 6.5(a) also shows a hysteresis in its phase transition temperature. The thermal diffusivity shows far less consistent behavior on heating and cooling than the electrical properties. In the high temperature phase there is a 10% discrepancy between the heating and cooling data. The phase transition range is extended on cooling over a 15 K range. The low temperature data shows a more significant discrepancy between the heating and cooling data.

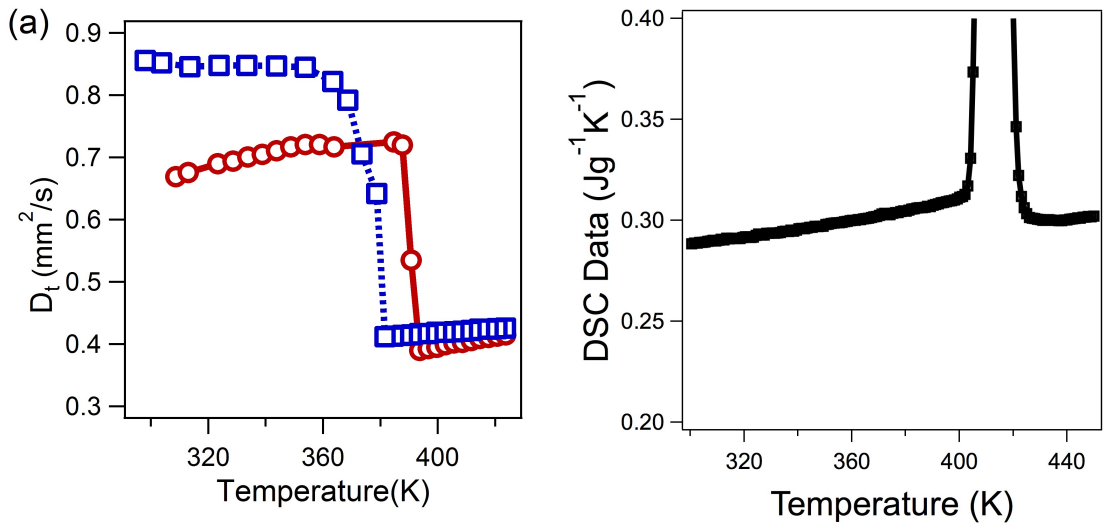

Figure 6.5: Thermal diffusivity (a) and Calorimetry data (b) for Ag_2Se measured on both heating and cooling.

In the context of identification of the order of the phase transition, the calorimetry was also discussed in Chapter 5.2 As Ag2Se has a first order phase transition, the peak in its calorimetry at 410 K represents an enthalpy of formation. At temperatures further below 400 K and above 420 K it is an accurate measurement of the heat capacity, and is used to calculate κ and zT. Between 400 K and 420 K the heat capacity used is that measured at 400 K — 0.317 J/gK.

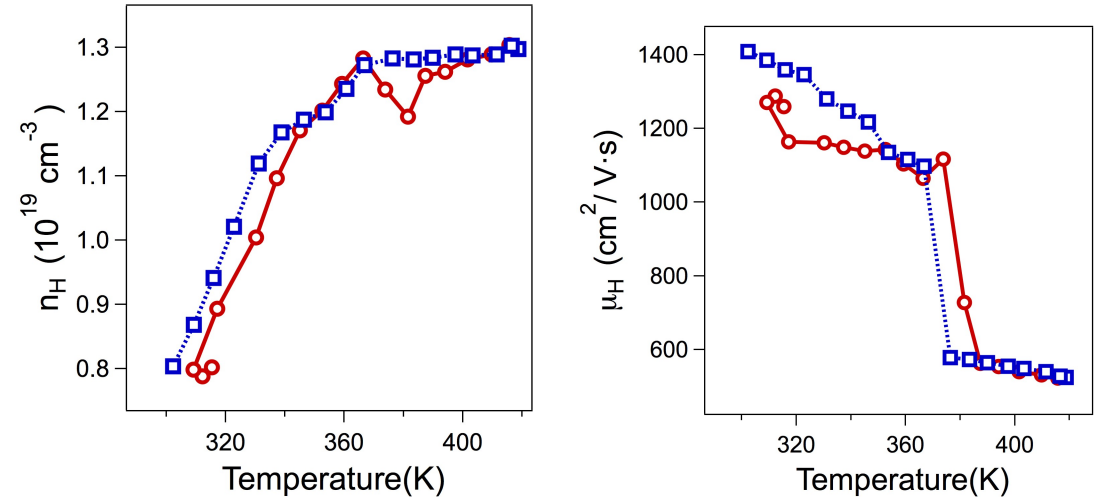

Figure 6.6: Hall Carrier Concencentration (a) and Hall Mobility (b) for Ag_2Se measured on both heating and cooling.

The Hall coefficient was measured concurrently with the electrical conductivity via the Van der Pauw method at 2 Tesla. The Hall carrier concentration (Figure 6.6(a)) and Hall mobility (Figure 6.6(b)) were thereby determined on heating and cooling. The Hall carrier concentration of Ag_2Se varies smoothly through the phase transition. This suggests that the band curvature (*i.e.*, effective mass) and the doping level are not altered measurably by the structural changes of the phase transition. The Hall mobility decreases by 50% through the phase transition. This is consistent with a sudden increase in the ion disorder and conductivity leading to increased scattering of electrons. It also explains the decrease in electrical conductivity observed at the phase transition temperature. Pardee and Mahan suggested that a steady Arrhenius increase in ion conductivity is observed due to Frenkel defect formation in both type I and type II super-ionics [151]. Such defect formation in Ag_2Se may alter the carrier concentration by localizing electrons more or less than the ground state sites. This would be indicated by a difference in Ag ion effective valency.

Below 360 K, the cooling Hall carrier concentration increases steadily with temperature; over the same range Seebeck decreases steadily. As the Hall carrier concentration become constant, so does the Seebeck coefficient. The data was of insufficient quality to prove this connection as causal. The Seebeck coefficient shows a 15% decrease from the low temperature to the high temperature phase, despite no measured shift in the carrier concentration. This data is inconsistent with the band model advanced in equation 6.5.

The total thermal conductivity of Ag_2Se is decreased by a factor of two in the disordered high temperature phase as compared to the ordered low temperature phase, see Figure 6.7(a). The Lorenz number of $L = 1.8 \times 10^{-8}\,W\Omega K^{-2}$ was used to calculate the electronic portion of the thermal conductivity. This quantity is taken from Day *et. al*'s [46] single parabolic band model of data from their samples and literature samples. From this Lorenz number κ_e and κ_L may be calculated. The lattice thermal conductivity of Ag_2Se decreases only slightly as the temperature increases through the phase transition temperature, indicating that the majority of the change in total thermal conductivity is due to the decrease in electrical conductivity, see Figure 6.7(a).

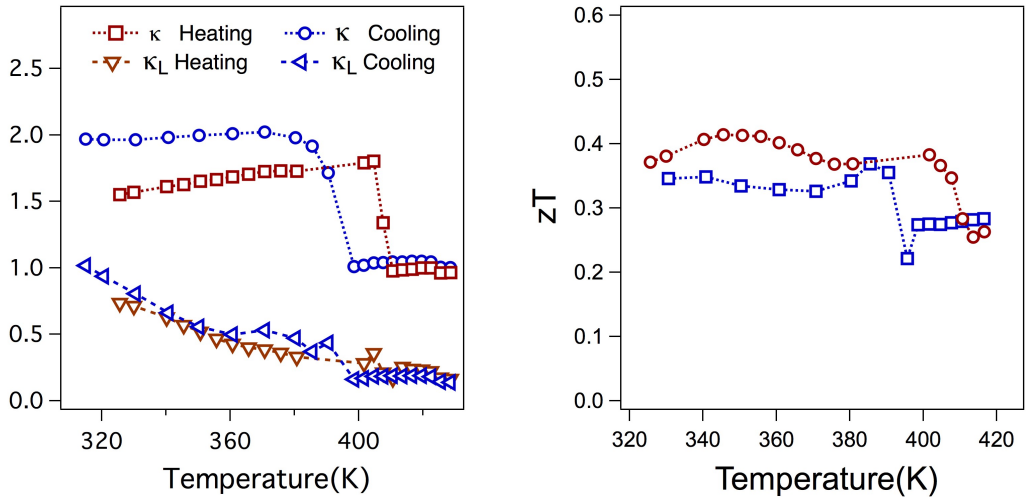

Figure 6.7: Left: Measured total and modeled lattice thermal conductivity of Ag_2Se. Right: zT of Ag_2Se. The zT in the ordered phase is markedly higher than the zT in the disordered phase.

The resulting lattice thermal conductivity is 0.35 W/mK below the phase transition temperature and 0.25 W/mK above it. This indicates that the Lorenz number of Day *et. al* is correct.

From the transport data presented above, the zT of Ag_2Se was determined on both heating and cooling, see Figure 6.7(b) Where necessary corrections to the temperature were made to align the phase transitions of all transport properties. In the calculated range between 320 K and 420 K zT is bound between 0.3 and 0.4, and it decreased upon transition to the disordered phase. The decrease in zT is 30%, which is consistent with the anomalous 15% decrease in the Seebeck coefficient at the phase transition temperature as zT varies with Seebeck squared. What explains this anomalous enhancement in Seebeck and zT?

One possible explanation would be a decrease in m^* from the ordered to the disordered phase. By equation 6.5 decreasing m^* should result in a decreased Seebeck coefficient. However, the band structure model of Day *et al.* suggests a moderate *increase* in m^* from the ordered to the disordered phase, see Figure 6.8(b). Such an increase is not compatible with the observed decrease in Seebeck coefficient. Day *et. al* suggest that the increase is from $0.2m_e$ to $0.3m_e$, but the error bars on their fit are

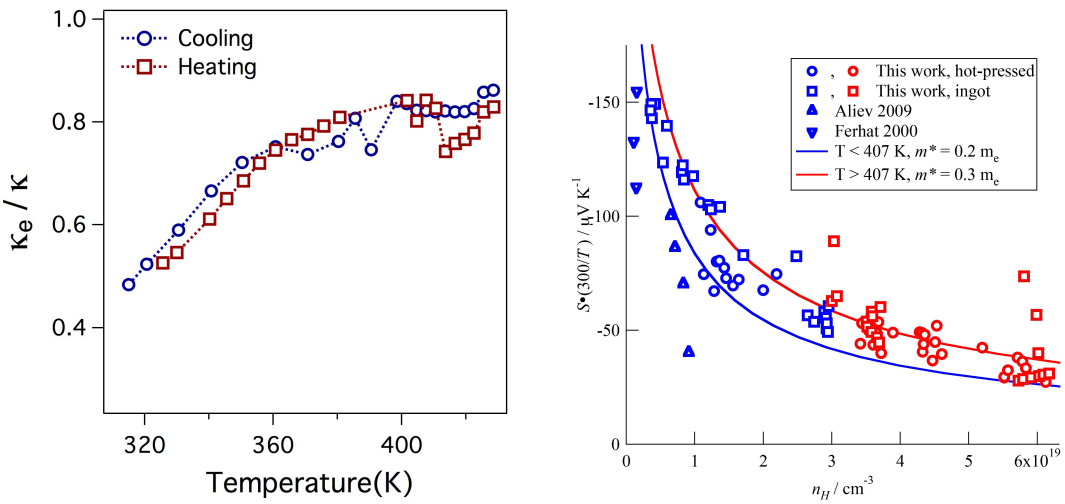

Figure 6.8: The ratio (a) of κ_E to κ is nearly identical on either side of the phase transition.
Pisarenko plot (b) for Ag_2Se. The disorder phase has a slightly larger m^* than the ordered phase. Modified version of Figure 2a in Day*et al.* [46] Courtesy of Tristan Day

such that the increase may be much smaller even than that.

Thermoelectric performance can also improve a more favorable portion of thermal transport due to electrons rather than the lattice; this is certainly possible given the decrease in κ_L observed, see Figure 6.7(a). The formula for $zT = \sigma\alpha^2/\kappa T$ can be reformulated in terms of L and κ_e as:

$$zT = \frac{\alpha^2}{L}\frac{\kappa_e}{\kappa} \tag{6.6}$$

With the contribution due to α discussed above and L varying significantly only for large changes in the Fermi level, the remaining contribution can be expressed as $\frac{\kappa_e}{\kappa}$. This term varies by less than 5% through the phase transition temperature, see Figure 6.8(a). This indicates that the enhancement in zT is entirely due to the enhancement in α noted above.

The enhancement in zT and α requires an alternate explanation from the single parabolic band model. More complex band effects such as band convergence [153] or resonant impurities [77] might be considered to explain the behavior. However,

these features are inconsistent with the constant n_H observed and the near constant m^* [154]. This suggests that an alternate explanation for the Seebeck and zT enhancement is required. This explanation must in some way be beyond that which even complex band structure modeling can capture. Over the next two chapters I will develop that explanation: co-transport of entropy associated with the order process leads to enhanced Seebeck and zT.